doi: 10.3969/j.issn.0490-6756.2017.04.018

$CuAlSe_2$ 在高压下结构、弹性、热学性质的第一性原理计算

周　梦[1]，卢志鹏[1,2]，陶应奇[1]，黄　鳌[1]，周　乐[3]，周晓云[1]，胡翠娥[4]
(1. 武警警官学院数学与物理学系，成都 610213；2. 中国工程物理研究院化工材料研究所，绵阳 621900；
3. 哈尔滨理工大学材料与科学工程学院，哈尔滨 150040；4. 重庆师范大学物理与电子工程学院，重庆 400047)

摘　要：本文中我们运用第一性原理平面赝势密度泛函理论，研究了四方晶体 $CuAlSe_2$ 的结构、弹性性质以及热力学性质. 首先通过状态方程拟合找到零温零压时的平衡体积、晶格常数、体弹模量 B_0 以及其对压强的一阶导数 B_0'. 接着分析了相对晶格常数 a/a_0、c/c_0 以及相对体积 V/V_0 随压强的变化趋势. 我们也研究了弹性常数随压强增大的变化趋势. 计算也表明在 15 GPa 以前 $CuAlSe_2$ 的弹性常数都满足力学稳定性，在 15 GPa 以前都不发生相变，与实验结果相吻合. 在零温零压下我们计算得到的弹性常数和体弹模量和其它理论值实验值都比较符合. 然后根据准谐德拜模型，我们分析了热膨胀系数以及比热容随压强和温度的变化关系. 最后我们分析了 $CuAlSe_2$ 晶体在零温零压和高压下的态密度图，简单了解了一下电子结构的变化情况.

关键词：密度泛函理论；高压性质；电子结构；$CuAlSe_2$
中图分类号：O521+.2　　**文献标识码**：A　　**文章编号**：0490-6756(2017)04-0771-10

Elastic and electronic properties of $CuAlSe_2$ under pressure: a first-principles study

ZHOU Meng[1], *LU Zhi-Peng*[1,2], *TAO Ying-Qi*[1], *HUANG Ao*[1],
ZHOU Le[3], *ZHOU Xiao-Yun*[1], *HU Cui-E*[4]
(1. Department of Mathematics and Physics, Officers College of People's Armed Police Force, Chengdu 610213, China;
2. Institute of Chemical Materials, China Academy of Engineering Physics(CAEP), Mianyang 621900, China;
3. School of Material Science and Engineering, Harbin of Science and Technology, Harbin 150040, China;
4. College of Physics and Electronic Engineering, Chongqing Normal University, Chongqing 400047, China)

Abstract: We employ the first-principles plane wave method in the frame of density functional theory (DFT) to investigate the equilibrium lattice structure, the mechanic, thermodynamic and electronic properties of $CuAlSe_2$ compound. The lattice constants, the bulk modulus B_0 and its pressure derivative B_0' are calculated. Based on the quasi-harmonic Debye model, we also obtain thermal expansion coefficient. It is noteworthy that the variation tendencies of these parameters are investigated detailedly or in detail with pressure. In addition, we also calculate the elastic constants of $CuAlSe_2$ compound. Results show that the elastic constants C_{11}, C_{33}, C_{12} and C_{13} increase with increasing pressure, whereas the influences of pressure on elastic constant C_{44} and C_{66} are not obvious. The calculated elastic constants satisfy the mechanical criterion until the pressure grows to more than 15 GPa, which suggests the structure

收稿日期：2017-05-17
基金项目：国家自然科学基金青年科学基金(11502244)
作者简介：周梦(1990－)，女，主要研究领域为第一性原理计算.
通讯作者：胡翠娥. E-mail: cuiehu@126.com

phase transition of $CuAlSe_2$ may be happened. We also investigate the shear sound velocity V_S, longitudinal sound velocity V_L, and Debye temperature Θ_E from our elastic constants, as well as the thermodynamic properties from quasi-harmonic Debye model. We obtain the dependence between the heat capacity C_v and pressure, and the same as thermal expansion coefficient α. At last, the pressure dependences of band structures and density of states are also investigated, which shows that the value of TDOS decreases with the increase of the pressure.

Keywords: Density functional theory; Elastic properties; Electronic properties; Thermodymanic properties

1 Introduction

The kinds of known ternary compounds exhibit diverse physicochemical properties and their chalcopyrite structure may be obtained from the zinc-blende structure by ordering the two cation sublattices[1]. For the family of materials, many interests are focus on the applications in nonlinear optics, photovoltaic optical detectors and solar cells[2-7]. As one of the known ternary compounds, $CuAlSe_2$, which belongs to the family of chalcopyrite, is a p-type semiconductor with a wide direct band gap at room temperature[8]. This feature makes $CuAlSe_2$ a promising application in the areas of light emitting diodes [9, 10].

Early in 1992, Morita and Narusawa found $CuAlSe_2$ thin film is blue by MBE (Molecular beam epitaxy)[11]. And then, several experimental studies carried on the structural, electronic and optical properties of $CuAlSe_2$[12, 13]. Jaffe and Zunger used the potential-variation mixed-basis (PVMB) approach to study the chemical trends in the electronic structure of $CuAlSe_2$[10]. Azuhata *et al*. did the similar work by measuring the first-order and the second-order Raman spectra[14]. Eifler *et al*. studied experimentally the zone-center phonon frequencies and the two-phonon spectra by measuring the Infrared and Raman spectra of $CuAlSe_2$[15]. These early studies were carried on the properties of $CuA1Se_2$ at ambient pressures. However, high-pressure studies of the $CuA1Se_2$ structure have attracted considerable attention due to their phase transition and electronic properties.

In experiments, Roa *et al*. studied the high-pressure properties of $CuAlSe_2$, and the chalcopyrite compound $CuAlSe_2$ was characterized by energy dispersive X-ray Diffraction (XRD) up to 25 GPa. They concluded that the pressure-induced first-order phase transition from the chalcopyrite structure to the cubic structure is observed at 12.4 GPa [16]. The ternary chalcopyrite compounds $CuAlSe_2$ were studied up to 14.8 GPa in a diamond anvil cell using energy dispersive X-ray diffraction (EDXRD) by Kumar *et al* [17]. In the terms of optical experiment, Roa *et al*. investigated the optical absorption edge and the Raman active modes of $CuAlSe_2$ as a function of pressure up to 30 GPa [18]. Then, Alonso *et al*. determined the dielectric tensor components of $CuAlSe_2$ in the energy range between 1.4 to 5.2 eV at room temperature by spectroscopic ellipsometry [19].

On the theoretical side, Jayalakshmi *et al*. studied the electronic and structural properties of the chalcopyrite $CuAlSe_2$ by using the first principle self-consistent tight binding linear muffin-tin orbital (TB-LMTO) method within the local density approximation [20]. The structure phase transition from bct structure (chalcopyrite) to cubic structure (rock salt) was observed at about 14.4 GPa. At the same time, they also studied the band gap value according to band structure, which was consistent with the experiment results. Besides, Maeda *et al*. systematically studied electronic structures of chalcopyrite-type $CuAlSe_2$ by first principles calculations using a plane-wave pseudopotential method within a density functional formalism [21]. In other aspect, Reshak and Auluck presented results of the band structure and density of states for the chalcopyrite

compounds $CuAlSe_2$ using the state-of-the-art full potential linear augmented plane wave (FP-LAPW) method [22]. Furthermore, Abdellaoui *et al*. obtained the elastic constants of $CuAlSe_2$ using FP-LMTO (full potential linear muffin-tin orbital), which calculated theoretically for the first time [23]. They also proposed that the phase transition pressure between the rocksalt and chalcopyrite structure phases of $CuAlSe_2$ is 8.89 GPa by calculating the thermal properties. In practice, the electronic, bonding and elastic properties are important because they can provide a deep insight into the inner properties of a material, and are also essential for its possible applications. High-pressure studies of these chalcopyrite semiconductors also have attracted considerable attention due to their phase transition and electronic properties. Thus in this work, we aim at providing more useful information by density functional calculations. In Sec. 2, the theoretical method is introduced and the computation details are given. Some results and discussion are presented in Sec. 3. Finally, the summary of our main results is given in Sec. 4.

2 Theoretical method and calculation details

In the electronic structure calculations, we employ the ultrasoft pseudopotential density functional theory method together with both the generalized gradient approximation (GGA) proposed by Perdew *et al*. [24] and the local density approximation (LDA) proposed by Vosko *et al*. [25] for exchange-correlation potentials. A plane-wave basis set with energy cut-off 880 eV is applied. For the Brillouin-zone sampling, we use the $3\times3\times4$ Monkhorst-pack mesh [26]. The self-consistent convergence of the total energy is 1.0×10^{-6} eV/atom, the maximum ionic force to 0.05 eV/Å, and the maximum stress to 0.1 GPa. These parameters are carefully tested. It is found that these parameters are sufficient to a well-converged total energy. All these electronic structure calculations are implemented through the CASTEP code [27]. By applying the method, we have investigated successfully the thermodynamic properties of several materials [28-30].

3 Results and discussion

3.1 Structural properties

For the tetragonal structure $CuAlSe_2$, the initial structural model is built according to previous available lattice parameters a and c. In its unit cell, Cu atom set at position (0, 0, 0), the atom of Al at position (0, 0, 0.5), and Se at position (z, 0.5, 0.5). We determined the static equilibrium structure by seeking for the minimum energy of the crystal. In other words, the most stable ground state structure of $CuAlSe_2$ can be found by the total energy electronic structure calculations over a wide range of primitive cell volumes V, i.e., from $0.7V_0$ to $1.2V_0$, where V_0 is the zero pressure equilibrium primitive cell volume. The detailed calculated procedures as follows: in the first step, for a given V, a series of different axial ratio c/a are taken to calculate the total energies E, and then minimized the total energy with the ratio c/a. This procedure is repeated over a wide range of V. Finally, we obtained the equilibrium parameters a, c, and c/a of $CuAlSe_2$ by fitting the calculated energy-volume (E-V) data to the third-order Birch-Murnaghan equation of state (EOS) [31],

$$\Delta E(V)=E-E_0=B_0V_0\left[\frac{V_0}{V_0}+\frac{1}{1-B_0'}+\frac{V_n^{1-B_0'}}{B_0'(B_0'-1)}\right] \tag{18}$$

where and V_0 are the zero temperature equilibrium energy and cell volume, B_0 and B_0' are the bulk modulus and its pressure derivative, respectively.

In Tab. 1, we list our results together with the available experimental data and other theoretical results. Obviously, the obtained lattice constants from the GGA method are better than those from the LDA methods. The three pseudopentials of norm-conserving (NC), ultrasoft and OTF are applied in our calculation. In case for GGA method, the obtained lattice constants $a(c)$ based on the three pseudopentials deviate 0.089%

(0.94%), 0.25% (1.50%) and 0.86% (0.01%) from its experimental values, respectively. But in the case for LDA calculations, the obtained corresponding errors are 0.94%, 1.50% and 0.01% for a, and 0.74%, 0.16% and 0.05% for c, respectively. It is obvious that the results from GGA and NC seem to be the best. Its lattice constants and the internal parameter of $CuAlSe_2$ are consistent well with other theoretical and experiment results. So we will investigate the mechanical and electronic properties of $CuAlSe_2$ with this method in the following.

Based on the GGA and NC (norm-conserving) methods, we calculated the crystal coordinate z, bulk modulus B_0 and pressure derivative B_0', which are also listed in Tab. 1. Results show that the obtained crystal coordinate $z=0.26$ agrees well with the results by Abdellaoui *et al* [23]. The obtained bulk modulus $B_0 = 77.24$ GPa is also in good agreement with other calculated results (71.15 [20], 85 [17], 76.03 GPa [23]). In addition, its pressure derivative $B_0' = 3.58$ is also consistent with the conclusion of Abdellaoui *et al* [23]. In fact, these excellent results indicate support for the reliability of the first-principles calculations presented here.

Tab. 1 Calculated equilibrium lattice parameters of $CuAlSe_2$, together with the experiment data and other theoretical results.

	a/Å	c/Å	c/a	z	B_0(GPa)	B_0'
GGA(Norm-conserving)	5.611	11.003	1.961	0.26	77.24	3.58
LDA(Norm-conserving)	5.557	10.981	1.976			
GGA (Ultrasoft)	5.592	11.063	1.978			
LDA (Ultrasoft)	5.485	10.883	1.984			
GGA (OTF)	5.558	11.009	1.981			
LDA (OTF)	5.500	10.905	1.983			
Other calculations[a](LMTO)	5.47	10.90	1.99	0.245	76.03	3.96
Other calculations [b](TB-LMTO)	5.6099	10.9578	1.953		71.15	
Other calculations[c](FP-LAPW)	5.602	10.946	1.954			
Exp. (EDXRD)[d]	5.61	10.90	1.943		85	
Exp. (PVMB) [e]	5.606	10.90	1.944			

a. Obtained from FP-LMTO code [23]; b. Obtained from TB-LMTO code [20]; c. Obtained from FP-LAPW code [22]; d. Obtained from the X-Ray diffraction measurements [17]; e. Obtained from the PVMB measurements [9].

The pressure dependences of the normalized lattice constants a/a_0, c/c_0, and the normalized cell volume V/V_0 of $CuAlSe_2$ are illustrated in Fig. 1, where a_0, c_0 and V_0 are the zero pressure equilibrium structure parameters. It is shown that, as the applied pressure increases from 0 to 14 GPa, the ratio c/c_0 (0.991%, 0.983%, 0.976%, 0.969%, 0.963%, 0.958%, 0.953%) decreases quickly, and its downward trend is more quick than that in a/a_0 (0.991%, 0.984%, 0.977%, 0.971%, 0.965%, 0.960%, 0.955%), indicating that the compression along c-axis is larger. However, there is no experimental data to be compared with our results at present.

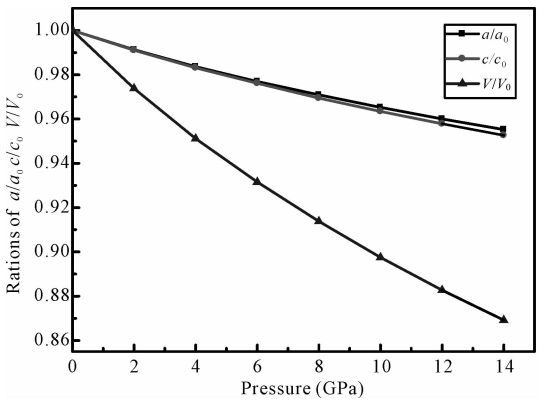

Fig. 1 The calculated normalized parameters a/a_0, c/c_0, and the normalized cell volume V/V_0 as a function of pressure at $T=0$ K

3.2 Elastic properties

We list our calculated elastic constants and

aggregate elastic modulus B, shear modulus G, B/G, Poisson ratios σ, acoustic velocities V_L and V_S (km/s) and elastic Debye temperature Θ_D of tetragonal structure $CuAlSe_2$ at 0 K and 0 GPa in Tab. 2. It can be seen clearly that our results are in agreement with the other theoretical and experimental data, which indicates that our results are reasonable. In addition, from the Eq. (9), the bulk modulus B_0 (in Tab. 2) obtained by our elastic constants is 71.93 GPa, which is consistent with the value estimated by fitting the E-V data mentioned above.

Tab. 2　Calculated elastic constants C_{ij} (GPa), bulk modulus B(GPa) of $CuAlSe_2$ at 0 K and 0 GPa, in comparison with the experimental data.

	C_{11}	C_{33}	C_{44}	C_{66}	C_{12}	C_{13}	B
Present	96.511	95.354	43.635	44.920	58.355	60.580	71.93
Cal.	102.918[a]	106.072[a]	46.058[a]	42.935[a]	60.924[a]	62.736[a]	76.03[a] 71.15[a]
Exp.							85[b,c]

a. Obtained from FP-LMTO code [23]; b. Obtained from the X-Ray diffraction measurements [17]; c. Obtained from the X-Ray diffraction measurements[16].

In Tab. 3, under a wide range of pressure (0-14 GPa), the elastic constants of $CuAlSe_2$ in different vegetation: C_{11}, C_{33}, C_{12}, C_{13} increase with the increasing pressure. While the elastic constants C_{44} and C_{66} remain nearly unchanged with the increasing pressure, which also can be observed from Fig. 2. It is also noted in Tab. 3 that $C_{11} > C_{33}$ in the whole range of pressure, which predicts that the atomic bonds along the {100} planes between nearest neighbors are stronger than those along {001} planes.

Tab. 3　Calculated elastic constants C_{ij} (GPa), bulk modulus B (GPa), shear modulus G (GPa), B/G, Poisson ratio σ, acoustic velocities, and V_L and V_S (km/s), and Deybe temperature Θ_D (K) of $CuAlSe_2$ under pressure P(GPa).

P	0	2	4	6	8	10	12	14	15
C_{11}	96.51	106.24	113.67	122.76	130.05	138.93	145.97	155.12	156.98
C_{33}	95.35	103.82	112.47	120.94	127.48	134.30	141.72	149.00	148.71
C_{44}	43.63	44.05	44.25	44.26	44.33	44.67	45.79	46.38	49.08
C_{66}	44.92	44.86	44.59	45.50	45.92	46.51	46.80	47.40	57.97
C_{12}	58.35	68.07	76.86	86.44	94.89	104.89	113.51	123.21	124.12
C_{13}	60.58	70.23	79.43	89.49	97.72	107.58	115.74	124.86	127.15
B	71.93	81.48	90.14	99.70	107.59	116.72	124.84	133.87	135.46
G	30.84	30.82	30.41	30.16	29.78	29.40	29.19	29.09	30.63
B/G	2.33	2.64	2.96	3.31	3.61	3.97	4.28	4.60	4.42
σ	0.31	0.33	0.35	0.36	0.37	0.38	0.39	0.40	0.39
V_L	5.90	6.06	6.18	6.33	6.43	6.56	6.67	6.80	6.53
V_S	3.08	3.04	2.98	2.94	2.89	2.85	2.82	2.79	2.72
Θ_D	292.38	291.70	289.28	287.66	285.31	283.04	281.56	280.63	346.95

For a tetragonal crystal, the mechanical stability leads to restrictions on the elastic constants under pressure as follows [32]: $(\widetilde{C}_{11} + \widetilde{C}_{33} - 2\widetilde{C}_{13}) > 0, \widetilde{C}_{11} > 0, \widetilde{C}_{33} > 0, \widetilde{C}_{44} > 0, \widetilde{C}_{66} > 0, \widetilde{C}_{11} - \widetilde{C}_{12} > 0$, $(2\widetilde{C}_{11} + 2\widetilde{C}_{12} + \widetilde{C}_{33} + 4\widetilde{C}_{13}) > 0$, where $\widetilde{C}_{\alpha\alpha} = C_{\alpha\alpha} - P(\alpha = 1,3,4,6), \widetilde{C}_{12} = C_{12} + P, \widetilde{C}_{13} = C_{13} + P$. It is obvious from Tab. 3 that the elastic constants of $CuAlSe_2$ satisfy all of these conditions above at pressure P below 14 GPa. In order to further study, we try to add up to 15 GPa (in Tab.

3), and found that when $P>14$ GPa, , it suggests that its structure phase transition of $CuAlSe_2$ may be happened, which agrees with the experiment [20].

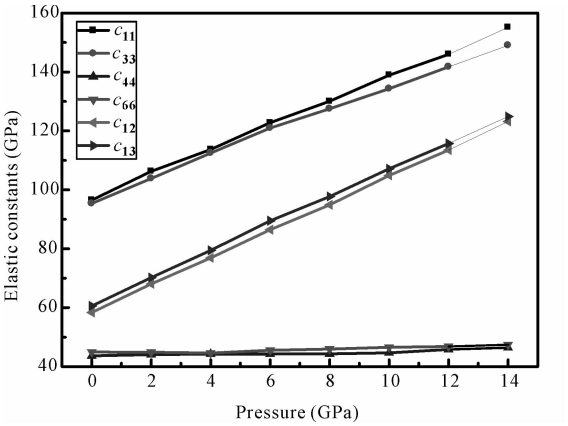

Fig. 2 Pressure dependencies of elastic constants of $CuAlSe_2$ at 0 K.

The bulk modulus of a material reflects its resistance to volume change, and the shear modulus describes the resistance to shape change. These two parameters closely related to the mechanical performance of a material [33]. From Tab. 3, we can find that the bulk modulus B increases gradually with the increase of pressure, indicating that tetragonal structure $CuAlSe_2$ becomes more difficult to compress with increasing pressure. In addition, a high (low) B/G value, which separates ductile and brittle materials, is about 1.75. In our work, from Tab. 3, the B/G ratio of tetragonal structure $CuAlSe_2$ is 2.33, hence describing the structure of this material as ductile. Tab. 3 also shows that the calculated values of B/G increases with increasing pressure, indicating that it becomes much harder with the increasing pressure.

According to the elastic constants obtained, we can also obtain the compressional and shear wave velocities of $CuAlSe_2$ under pressure. We list them in Tab. 3, and the results of them are V_L = 5.90 km/s and V_S = 3.08 km/s at 0 GPa. It is shown that with the increasing pressure, the compressional wave velocities increases in Fig. 3. The shear wave velocity changes slowly with the elevated pressure, and fluctuates inconspicuously at higher pressure. Unfortunately, there are no experimental data to be compared with our results.

The Debye temperature is an important parameter related to many physical properties of solids, such as specific heat, elastic constants, and melting temperature. From the calculated Debye temperature in Tab. 3, we can clearly see that the Debye temperature decreases with the increasing pressure. Unfortunately, there is also no experimental and theoretical data for our comparison.

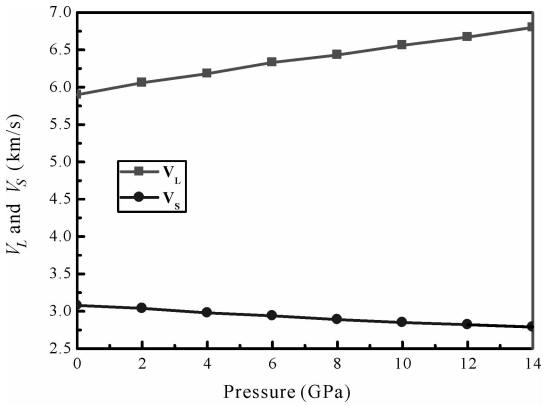

Fig. 3 The compressional and shear wave velocities of $CuAlSe_2$ as a function of pressure at $T=0$.

3.3 Thermodynamic properties

The thermal expansion coefficient and specific heats C_v are the important reference to predict material properties, especially for the thermodynamic properties. We present the variations of the thermal expansion α and specific heats C_v with temperature and pressure in Figs. 4 and 5 respectively. Seen from the Fig. 4, at a given pressure, α increases exponentially at low temperatures and gradually approaches a linear increase at high temperature. As the pressure increases, the growth trend of α with temperature becomes smaller and smaller, especially at high temperature. However, at a given temperature, α decreases drastically with the increasing pressure. When the pressure increase to above 10 GPa, the thermal expansion α of 600 K is just a little larger than that of 500 K and the curves of 400, 600 and 800 K seem to be consistent at high pressure, which means that the temperature dependence of

α is very small at high pressure and high temperature.

In Fig. 5, we can find that the C_v rises rapidly with the temperature at low temperatures, but at high temperatures, the anharmonic effect on C_v is suppressed, C_v converges slowly to the Dulong-Petit limit. It also shows that the effect of temperature on the special heat capacity C_v is much larger than that of pressure.

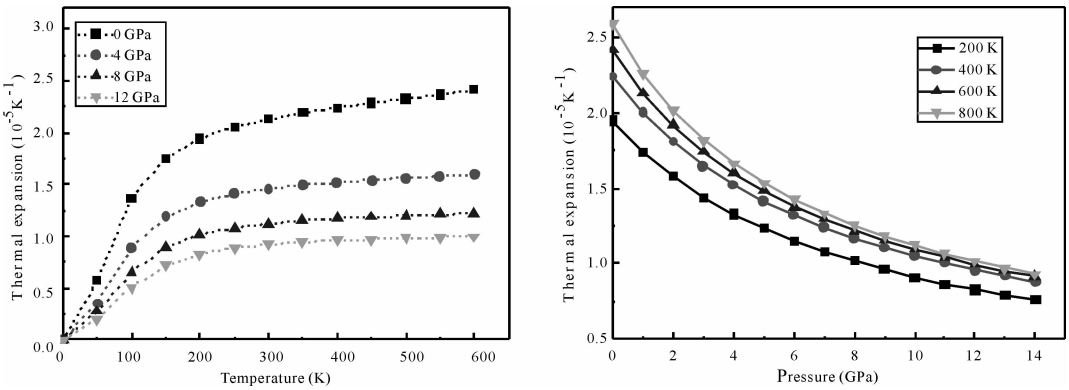

(a)　　(b)

Fig. 4　Thermal expansion versus temperature and pressure of $CuAlSe_2$.

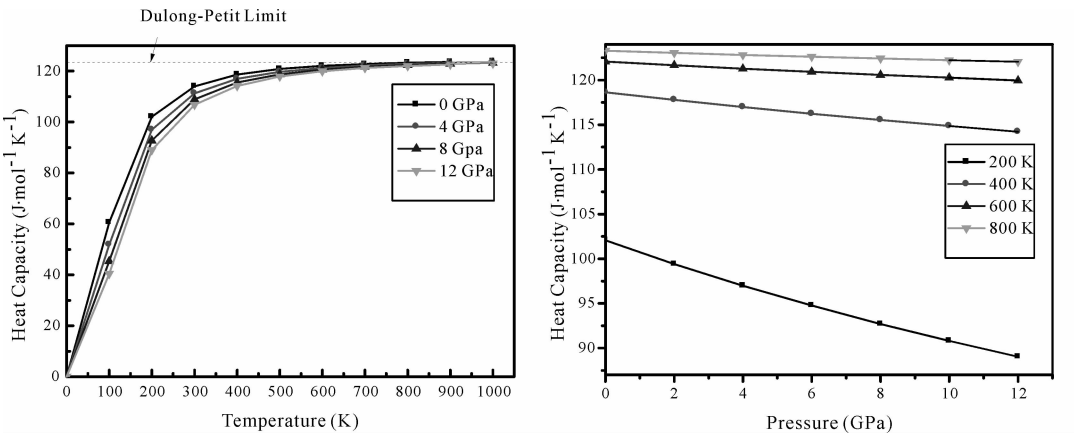

(a)　　(b)

Fig. 5　The heat capacity C_v of $CuAlSe_2$ as a function of temperature T at several pressures.

3.4　Electronic structure

One can see from Fig. 6 that the bands below the Fermi level can be divided into three parts, i. e. the first part is located in the range of −14 to −12 eV (part Ⅰ); the second one is between −7 and −3 eV (part Ⅱ); the third one extends from −2 to the Fermi level (part Ⅲ). Apparently, in parts Ⅱ and Ⅲ, the bands located at around −13, −6 and −1 eV have a remarkably localized characteristic, but the others behave much dispersing. To find the reasons for these characters, we make an investigation to the calculated total density of states (TDOS) and partial density of states (PDOS), which are illustrated in Fig. 7. It is found that the bands at −6 eV come from the sharp hybridization among Se-3p and Al-3s orbitals; the bands at −13 and −1 eV mainly originate from Se-3s and Cu-3d state, respectively, a well-known state for its strongly localized characteristic. These origins give these bands a similar flat outer behavior. The bands below −12 eV in part Ⅰ result from the interaction between Se-3s and Al-3s, 3p; the bands above −7 eV in part Ⅱ derive largely from Se-3p, Cu-3d and Al-3s, 3p; while the bands in part Ⅲ are mainly composed by Cu-3d orbitals, together with contributions

from Se-3p. As is known, the s and p electrons are the outer electrons of Al and Se atoms, when these atoms are tetrahedrally coordinated with each other, they often form the sp^3 hybridization, which is a stronger orbital interaction and then leads to a dispersing behavior of the corresponding bands. But in part Ⅲ, some s electrons of Al atom have to contribute to form the Al-Se bond, which to some extent weakens the interaction between Se-3p and Al-3s, together with a lager electron population in this part, making the corresponding bands seem dense and not so much fluctuant. It is noticed that the top of the valence bands are chiefly occupied by Cu-3d, while the bottom of the conduction bands are mainly formed by Al-3s, 3p and Cu-4s, which means that when the electrons are excited, there is a larger possibility for them to transit from Cu-3d to Al-3s, 3p or Cu-4s, forming the absorbing edge of the measured optical spectral.

The calculated total density of states (TDOS) and partial density of states (PDOS) at high pressure are also illustrated in Fig. 7. It is found that: (1) The TDOS values become smaller when the pressure is increased, especially the value in the range of valance band, as well as the peak value of Cu-3d. Thus, we can predict that the obtained peak is due to 3d of Cu. (2) The peak of Al-3s in the conduction band moves slowly away from it. Therefore, the DOS peak near 2.5 eV moves right slowly.

4 Conclusions

We have investigated the electronic structure and elastic properties of $CuAlSe_2$ under pressure in the frame of the density functional theory (DFT). The calculated lattice parameters of $CuAlSe_2$ at zero pressure and zero temperature from GGA and norm-conserving are in agreement with the available experimental and theoretical data. According to the electronic structure calculations, the pressure dependence of the lattice

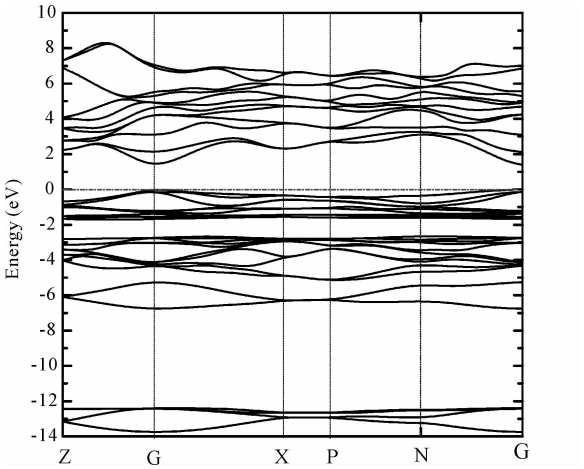

Fig. 6 Band structure of $CuAlSe_2$: dotted line at 0 eV refers to the Fermi energy level.

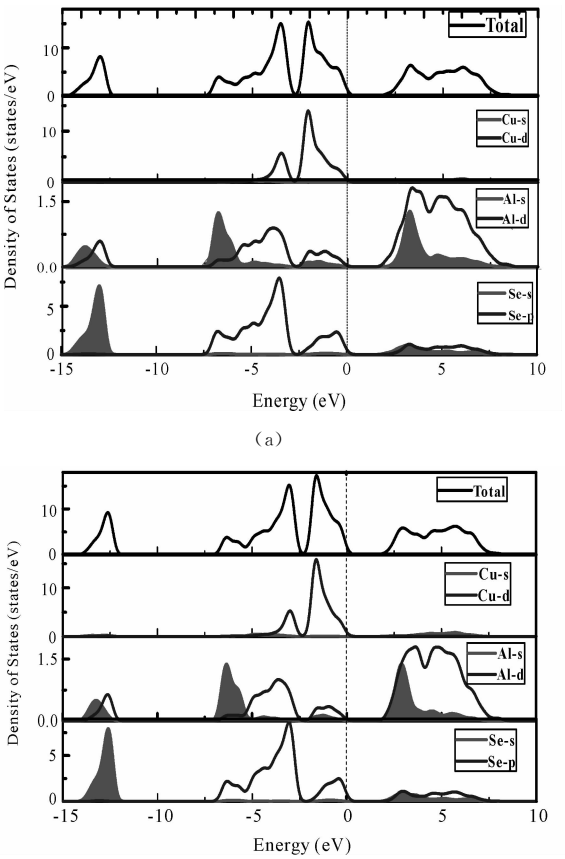

Fig. 7 Calculated total and partial density of states of structure $CuAlSe_2$ at 0 GPa (a) and 10 GPa (b).

constants and cell volume are analyzed, and results show that the compression along the *c*-axis is larger than the *a*- and *b*-axis.

The calculated elastic constants and bulk modulus are in agreement with the available experimental and other theoretical data. It is found that, $CuAlSe_2$ is mechanically anisotropic in the

range of 0 to 15 GPa, in which the elastic constants C_{11}, C_{33}, C_{12}, C_{13} increase, and the variation of elastic constants C_{44} and C_{66} is not obvious as pressure increases. The computed ratio of B/G is larger than 1.75, indicating that $CuAlSe_2$ is a ductile crystal; the calculated Poisson ratio reveals that it is an ionic-covalent crystal.

We also have investigated the thermal properties of $CuAlSe_2$ by utilizing quasi-harmonic Debye model. The thermal calculations show that the thermal expansion coefficient is positively related to the temperature changes, and negatively related to the pressure varied. And the effect of temperature on the special heat capacity C_v is much larger than that of pressure.

Furthermore, we analyses the variety tendency of the TDOS and PDOS at high pressure. It is found that the TDOS values become smaller when the pressure is increased, especially the value of valance band, as well as the peak value of Cu-3d. Thus, we can predict that the obtained peak is due to 3d of Cu.

References:

[1] Pamplin B R, Kiyosawa T, Masumoto K. Ternary chalcopyrite compounds [J]. Prog Cryst Growth Charact, 1979, 1: 331.

[2] Birkmire R W, Dinetta L C, Lasswell P G, *et al*. High efficiency $CuInSe_2$ based heterojunction solar cells: fabrication and results [J]. Sol Cells, 1986, 16: 419.

[3] Wagner S, Shay J L, Migliorator P, *et al*. $CuInSe_2$/Cds heterojunction photovoltaic detectors [J]. Appl Phys Lett, 1974, 25: 434.

[4] Shirakata S, Murakami K, Isomura S. Electroreflectance studies in $CuGaS_2$ [J]. Jpn J Appl Phys, 1989, 28: 1728.

[5] Jaffe J E, Zunger A. Theory of the band-gap anomaly in ABC_2 chalcopyrite semiconductors [J]. Phys Rev B, 1984, 29: 1882.

[6] Fan Y X, Eckardt R C, Byer R L, *et al*. $AgGaS_2$ infrared parametric oscillator [J]. Appl Phys Lett, 1984, 45: 313.

[7] Bethune D S, Luntz A C. A laser infrared source of nanosecond pulses tunable from 1.4 to 22 μm [J]. Appl Phys B, 1986, 40: 107.

[8] Benchouk K, Benseddik E, ElMoctar C O, *et al*. New buffer layers, large band gap teneary compounds: $CuAlTe_2$ [J]. Eur Phys J Appl Phys, 2000, 10: 9.

[9] Azhnyuk N Y, Artamonov V V, Bodnar V I. Rman scattering in mixed $CuAl_{1-x}Ga_xSe_2$ crystals [J]. J Appl Spectrosc, 1985, 43: 1276.

[10] Jaffe J E, Zunger A. Electronic structure of the ternary chalcopyrite semiconductors $CuAlS_2$, $CuAlSe_2$, $CuGaSe_2$, and $CuInSe_2$ [J]. Phys Rev B, 1983, 28: 5822.

[11] Morita Y, Narusawa T. Charaterization of $CuAlS_2$ films grown by molecular beam epitaxy [J]. Jpn J Appl Phys, 1992, 31: 3802.

[12] Chichibu S, Shishikura M, Ino J, *et al*. Electrical and optical properties of $CuAlSe_2$ grown by iodine chemical vapor transport [J]. Appl Phys, 1991, 70: 1648.

[13] Andriesh A M, Syrbu N N, Iovu M S, *et al*. Infrared vibrational modes and anisotropy of the effective ionic charge in $CuAlSe_2$, $CuAlS_2$, and $CuGaSe_2$ crystals [J]. Phys Stat Sol B, 1995, 187: 83.

[14] Azuhata T, Terasako T, Yoshida K, *et al*. Lattice dynamics of $CuAlS_2$ and $CuAlSe_2$ [J]. Phys Rev B, 1996, 219: 496.

[15] Eifler A, Kudritskaya E A, Bodnar I V, *et al*. Infrared and Raman study of lattice vibrations of $CuAlSe_2$ single crystals [J]. J Phys Chem Solids, 2003, 64: 1983.

[16] Roa L, Chervin J C, Itie J P, *et al*. High-Pressure structural study of $CuAlS_2$ and $CuAlSe_2$ [J]. Phys Stat Sol B, 1999, 211: 455.

[17] Kumar R S, Sekar A, Victor N J, *et al*. Structural studies of $CuAlSe_2$ and $CuAlS_2$ chalcopyrites at high pressure [J]. J Alloy Comp, 2000, 312: 4.

[18] Roa L, Chervin J C, Chevy A, *et al*. Optical absorption and Raman scattering measurements in $CuAlSe_2$ at high pressure [J]. Phys Stat Sol B, 1996, 99: 198.

[19] Alonso M I, Pascual J, Garriga M, *et al*. Optical properties of $CuAlSe_2$ [J]. Appl Phys, 2000, 88: 1923.

[20] Jayalakshmi V, Davapriya S, Murugan R, *et al*. Electronic structure and structural phase stability of $CuAlX_2$ (X=S, Se, Te) under pressure [J]. J Phys Chem Solids, 2006, 67: 669.

[21] Maeda T, Takeichi T, Wada T. Systematic studies on electronic structures of $CuInSe_2$ and the other chalcopyrite related compounds by first principles

calculations [J]. Phys Stat Sol A, 2006, 203: 2634.

[22] Reshak H A, Auluck S. Electronic properties of chalcopyrite $CuAlX_2$ (X = S, Se, Te) compounds [J]. Solid State Commun, 2008, 145: 571.

[23] Abdellaoui A, Ghaffour M, Bouslama M, *et al*. Structural phase transition, elastic properties of chalcopyrite $CuAlX_2$ (X = S, Se, Te) [J]. J Alloy Comp, 2009, 487: 206.

[24] Perdew J P, Wang Y. Accurate and simple analytic representation of the electron-gas correlation energy [J]. Phys Rev B, 1992, 45: 13244.

[25] Vosko S H, Wilk L, Nusair M. Accurate spin-dependent electron liquid correlation energies for local spin density calculations: a critical analysis [J]. Can J Phys, 1980, 58: 1200.

[26] Monkhorst H J, Pack J D. Special points for Brillouin-Zone integrations. [J]. Phys Rev B, 1976, 13: 5188.

[27] Segall M D, Lindan P J D, Probert M J, *et al*. First-Principles simulation: ideas, illustrations and the CAETEP code [J]. Phys Rev B, 2002, 73: 2717.

[28] Chen X R, Zeng Z Y, Liu Z L, *et al*. Elastic anisotropy of ε-Fe under conditions at the Earth's inner core [J]. Phys Rev B, 2011, 83: 132102.

[29] Ao T G, Ying C, Zhao E J, *et al*. First principles studies on mechanical Properties of ZrB_3 and NbB_3 under high Pressure [J]. J Sichuan Uni: Nat Sci Ed (四川大学学报: 自然科学版), 2017, 54: 3.

[30] Zhan G F, Chen F Q, Zhu J, *et al*. Phase transition, elastic and thermodynamic properties of PtN_2 under high pressure from first-principles study [J]. J Sichuan Uni: Nat Sci Ed (四川大学学报: 自然科学版), 2016, 53, 6.

[31] Brich F. Finite elastic strain of cubic crystals [J]. Phys Rev B, 1947, 71: 809.

[32] Sin'ko V G, Smirnov A N. Ab initio calculations of elastic constants and thermodynamic properties of bcc, fcc, and hcp Al crystals under pressure [J]. J Phys: Condens Matter, 2002, 14: 6989.

[33] Pugh F S. Relations between the elastic moduli and the plastic properties of polycrystalline pure metals [J]. Philos Mag, 1954, 45: 823.